Design and control of multiphase interleaved boost converters-based on differential flatness theory for PEM fuel cell multi-stack applications

Phatiphat Thounthong, Pongsiri Mungporn, Damien Guilbert, Noureddine Takorabet, Serge Pierfederici, Babak Nahid-Mobarakeh, Yihua Hu, Nicu Bizon, Yigeng Huangfu, Poom Kumam

Design and Control of Multiphase Interleaved Boost Converters-Based on Differential Flatness Theory for PEM Fuel Cell Multi-Stack Applications

Phatiphat Thounthong[1,2*], Pongsiri Mungporn[1,3]

[1]*Renewable Energy Research Centre (RERC)*
[2]*Department of Teacher Training in Electrical Engineering, Faculty of Technical Education*
[3]*Thai-French Innovation Institute*
King Mongkut's University of Technology North Bangkok,
1518, Pracharat 1 Rd., Bangsue, Bangkok 10800, Thailand
e-mail: phatiphat.t@fte.kmutnb.ac.th , pongsiri.m@tfii.kmutnb.ac.th

Damien Guilbert[4,*], Noureddine Takorabet[4], Serge Pierfederici[5]

[4] *Université de Lorraine, GREEN, F-54000 Nancy, France*
[5] *Université de Lorraine, CNRS, LEMTA, F-54000 Nancy, France*
e-mail: damien.guilbert@univ-lorraine.fr, noureddine.takorabet@univ-lorraine.fr, serge.pierfederici@univ-lorraine.fr

Babak Nahid-Mobarakeh
Department of Electrical and Computer Engineering, *McMaster University*,
Hamilton, ON L8S 4L8, Canada
e-mail: babak.nahid@mcmaster.ca

Yihua Hu
Department of Electronics Engineering, University of York
York, YO10 5DD, U.K.
e-mail: yihua.hu@york.ac.uk

Nicu Bizon
Faculty of Electronics, Communication, and Computers, University of Pitesti,
Pitesti 110040, Romania
e-mail: nicu.bizon@upit.ro

Yigeng Huangfu
School of Automation, *Northwestern Polytechnical University,*
Xi'an 710072, China
e-mail: yigeng@nwpu.edu.cn

Poom Kumam
Center of Excellence in Theoretical and Computational Science (TaCS-CoE), Faculty of Science,
King Mongkut's University of Technology Thonburi (KMUTT),
126 Pracha-Uthit Road, Bang Mod, Thrung Khru, Bangkok 10140, Thailand
e-mail: poom.kumam@mail.kmutt.ac.th

*Corresponding Author: P. Thounthong (phatiphat.t@fte.kmutnb.ac.th) and D.Guilbert (damien.guilbert@univ-lorraine.fr)

***Abstract*—This article is focused on the development of an energy management algorithm applied to a multi-stack fuel cell (FC) system for DC microgrid applications. To guarantee the performance of the FC stacks, the current ripple is reduced by employing multiphase interleaved boost converters. A proposed advanced control technique of the multi-stack with multiphase converters for the proton exchange membrane (PEM) FCs is estimated based on a differential flatness approach, in which it can track the power demand in real-time. Furthermore, the differential flatness based-control can ensure the balance of the DC bus voltage of the DC microgrid when load disturbance occurs. The flatness-based energy management strategy is based on both inner current loops (control of the multi-stack PEMFC through their multiphase interleaved boost converters) and outer voltage loop (DC bus voltage regulation). Compared to classic PI controllers mainly based on the linearization of the system to obtain the transfer function (making complex its application), the flatness-based theory leans on time-domain making it easier its use for various applications while ensuring good performances. To validate the proposed control structure, an FC converter system (5 kW) is realized and validated in the laboratory. For hydrogen production, the methanol FC system has consisted of a reformer engine that changes water mixed methanol liquid into hydrogen to supply FC stacks (ME²Power Fuel Cell System: 50 V, 5 kW). The proposed control algorithm is tested experimentally by using a**

dSPACE controller board platform. Simulation and test bench results authenticate the excellent performance during load cycles in DC microgrid.

Keywords— DC microgrid; differential flatness control; Interleaved boost converter; fuel cell multi-stack; energy control.

NOMENCLATURE

Acronyms

FC	fuel cell.
PEMFC	proton exchange membrane fuel cell.
PI	proportional-integral.
PM	phase margin.

Roman Symbols

C_B	DC bus capacitance (F).
d	duty cycle.
e	error signal.
E_B	DC bus capacitive energy (J).
f_s	switching frequency (Hz).
i_{FC}	input fuel cell current (A).
i_L	inductor current (A).
i_{Load}	load current at the DC bus (A).
K_i	controller parameters.
K_p	controller parameters.
L	input inductance (H).
p_{FC}	fuel cell power (W).
p_{Load}	load power (W).
r_L	Resistive losses (Ω).
v_C	DC bus voltage of the microgrid (V).
v_{FC}	input fuel cell voltage (V).
u	inputs or control variables.
x	state variables (or state vector).
y	output vector (named in this article *flat outputs*).

Subscripts

c	command signal.
d	desired reference.
t	trajectory.

v	variable.

Greek Symbols

α	positive integers.
β	positive integers.
γ	positive integers.
ξ	damping ratio.
λ	stabilizing output (named in this article *control law*).
ω_n	natural frequency (rad.s^{-1}).

I. INTRODUCTION

Currently, proton exchange membrane fuel cell (PEMFC) is the fittest technology for DC microgrid applications since they offer compactness (i.e. high power density), and low operating temperature (enabling quick start-up), in comparison with other FC technologies [1],[2]. Nonetheless, they require the use of a noble-metal catalyst (i.e. platinum) leading up to the increase of their cost. The cost is not the only key issue but also the durability of PEMFC. Indeed, their limited durability impedes large-scale market penetration, both for automotive and stationary applications. Besides, for stationary applications, the expected durability is included between 60,000 and 80,000-hour. For this reason, the use of suitable power electronics and robust control algorithms for the optimal energy management of PEMFC systems plays a key role to make them more cost-effective and efficient [3-5].

An FC generator supplied by a hydrogen reformer needs to be linked through power electronic circuits (DC/DC or DC/AC) [6],[7]. In general, an FC stack requires a conventional boost converter (DC/DC converter) to transform the FC output low voltage v_{FC} to the high DC bus voltage v_C set-point, and also to smooth the FC supply current i_{FC}, as displayed in Fig. 1 [8-10]. In previous works reviewing DC-DC converter topologies for FC applications [11],[12], it has been emphasized that classic boost converters suffer from several disadvantages and cannot meet the expectations of DC-DC converters for FC applications. Indeed, classic boost converters feature limited voltage ratio (making them not fit for applications requiring high-voltage ratios such as DC microgrid and transportation), high current ripple by keeping the inductor small, and one single switch limiting their use for low-power applications. Furthermore, they are not available if a power switch failure occurs. As a result, the utilization of paralleling boost power circuits (called “multiphase”) with the interleaved switching approach may offer better efficiency, reliability in case of electrical failures [13-15]. Besides, these circuits enable extending their use to high-power applications, particularly interesting in developing high-power DC microgrids.

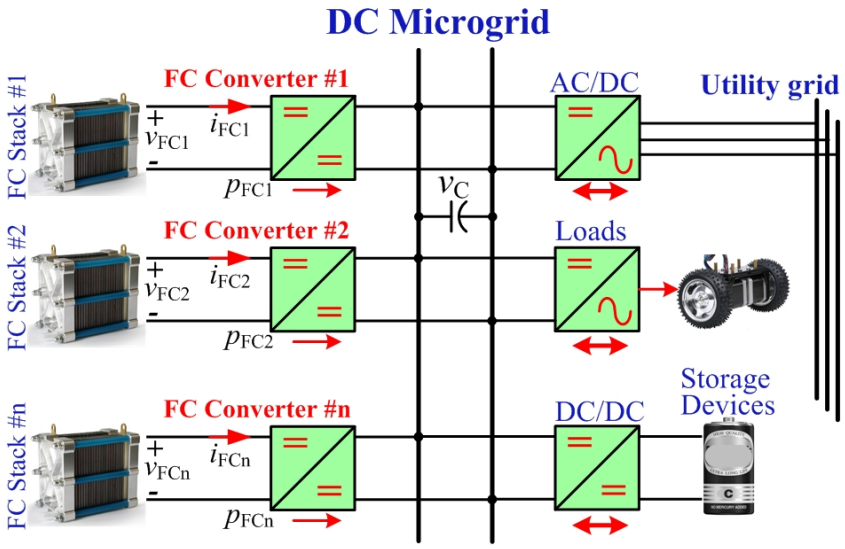

Fig. 1. FC/reformer power plant for DC microgrid applications.

Nevertheless, many technical barriers constrain PEMFCs energy-generating as a reliable energy source for DC microgrid applications. One restrictive issue is that PEMFCs supply low power and voltage at their outputs. Single PEMFC stack might not drive a load at DC bus through the interface converter. Moreover, to amplify the overall output power, to improve system reliability, and to accomplish robustness against system failures, there is a requirement for combining energy from multiple PEMFC stacks [16],[17]. In this work, as illustrated in Fig. 2, one proposes the multi-stack with multiphase interleaved boost converters for PEMFCs supplied by hydrogen reformer engine for the DC microgrid system, in which multiphase boost converters (here 2 phases) are coupled at the output of each stack (here 2 stacks), which are subsequently interfaced in parallel to distribute the load at the common DC bus. Two-phase interleaved boost converters have been chosen for experimental purposes. Indeed, the generation of their PWM gate control signals can be easily achieved by using a dSPACE controller board. From three phases, a microcontroller or FPGA board must be used to generate the PWM gate control signals due to the limited sampling period of dSPACE controller board [18].

In the literature, several works have been reported concerning the development of energy management for multi-stack fuel cell applications [19-21]. In [19], the authors have developed a rule-based energy management strategy for a multi-stack fuel cell system (based on a parallel architecture) and a battery system for automotive applications; whereas in [21], adaptive energy management strategy based on two different approaches (i.e. daisy chain and equal distribution) has been employed to manage a multi-stack fuel cell system combined with a battery system according to the requested power. In both works, the energy management strategy is validated in simulation but the regulation of the DC bus voltage has not been taken into consideration. In comparison, in [20], the authors have proposed energy and indirect sliding mode controllers applied to a multi-stack fuel cell system (based on a parallel architecture) and a supercapacitor module for transportation applications to regulate DC bus voltage and supercapacitor voltage as well. Simulation and experimental results are presented to validate the effectiveness of the proposed strategy.

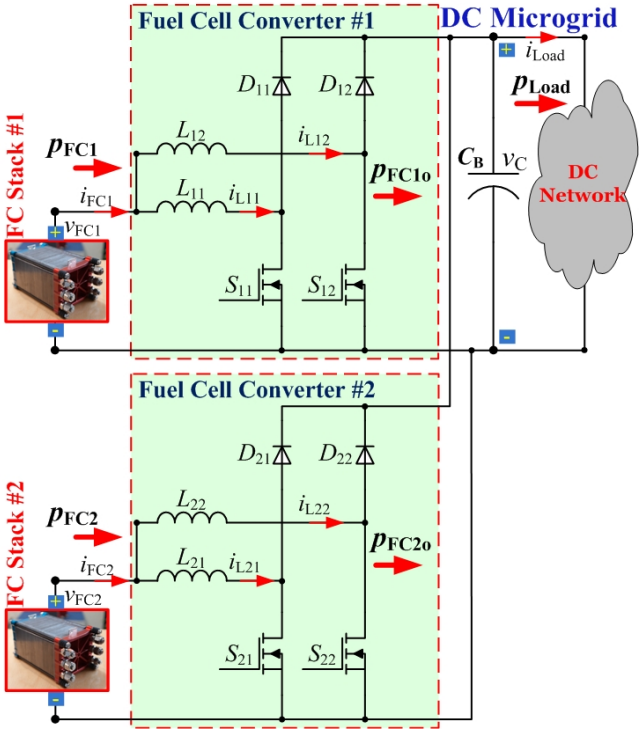

Fig. 2. Proposed two stack FC with two phase parallel boost converters for each stack for dc microgrid networks.

Generally, the difficulties in regulating boost converters lie in the existent external/internal disturbances and their nonlinear nature, and parameter variations [22],[23]. Unidentified fluctuations of both the input source voltage and the external load power demanded to degrade the performance of the compensators. Input source voltage fluctuations are an often–encountered circumstance that may occur from the utilization of PEMFC stacks. An effective control law must suddenly respond even under system disturbances. In the literature [20],[24-27], various approaches have been studied to stabilize the DC bus voltage (here, the most important variable) such as sliding mode [20],[25], modulated hysteresis [24], fuzzy logic [26], and observers and Lyapunov-based controllers [27]. These approaches have demonstrated their effectiveness in ensuring the stability of the DC bus for dynamic operations compared to classic linear proportional-integral (PI) controllers. It has to be noted that the DC bus voltage v_C of the classic boost DC/DC converter is of non-minimum phase (right-half plane zero), which constrains the compensator implementation since the dynamic system is unstable around the operating point [28]. Nevertheless, it has been demonstrated that the differential flatness based-control theory allows stabilizing to boost converter systems [29],[30]. For clarity, Fig. 3 displays an experimental evaluation of the differential flatness-based and classic (PI) control approaches, which sets a DC bus output voltage of 60 V in a four–phase boost converter (parallel interleaved switching) generated by a Li-Ion battery energy source to step an external load power demanded, as studied by Thounthong *et al*. [31]. In this work, the control of a hybrid energy system (photovoltaic system, FC system, and Li-ion battery module) is investigated by using two different control approaches. Indeed, the DC bus voltage is regulated through the use of a flatness-based controller (Fig. 3); whereas the different DC-DC converters connected to the sources are controlled through inner current loops-based on PI controllers. To realize a practical observation between the control approaches, the PI control parameters were set to achieve the optimum dynamics at a phase margin (PM) of 30° and 55°. Fig. 3 depicts the DC bus voltage regulations at

different compensators. It displays the DC bus voltage, the external load power, and the Li-Ion battery power. At t = 100 ms, the external load power is increased from 0 W to 300 W; one may examine that the differential flatness-based control depicts optimum response and excellent stability of the DC bus output voltage. Even though the dynamic response of the PI controller could be enhanced comparative to that revealed in Fig. 3, this operation comes at the risk of a stability margin: rising overshoot and signal fluctuation. Finally, compared to PI controllers where the design is based on frequency domain requiring the use of Laplace transform, the flatness-based theory is based on time-domain making it easier its application for different systems [31].

Based on the current literature where a few articles have been reported for the energy management of multi-stack fuel cell systems [19-21],[32] and the previous work on this topic [31], the main contribution of this article is to develop a flatness-based energy management strategy based on both inner current loops (multiphase interleaved boost converters) and outer voltage loop (DC bus voltage regulation) applied to a multi-stack PEMFC system. The control strategy has been developed and designed so that it can regulate the DC bus voltage while managing both multi-stacks PEMFC through their multiphase interleaved boost converter according to the load demand. Experimental tests have been carried out a suitable experimental test bench to validate the developed control strategy according to different dynamic load profiles.

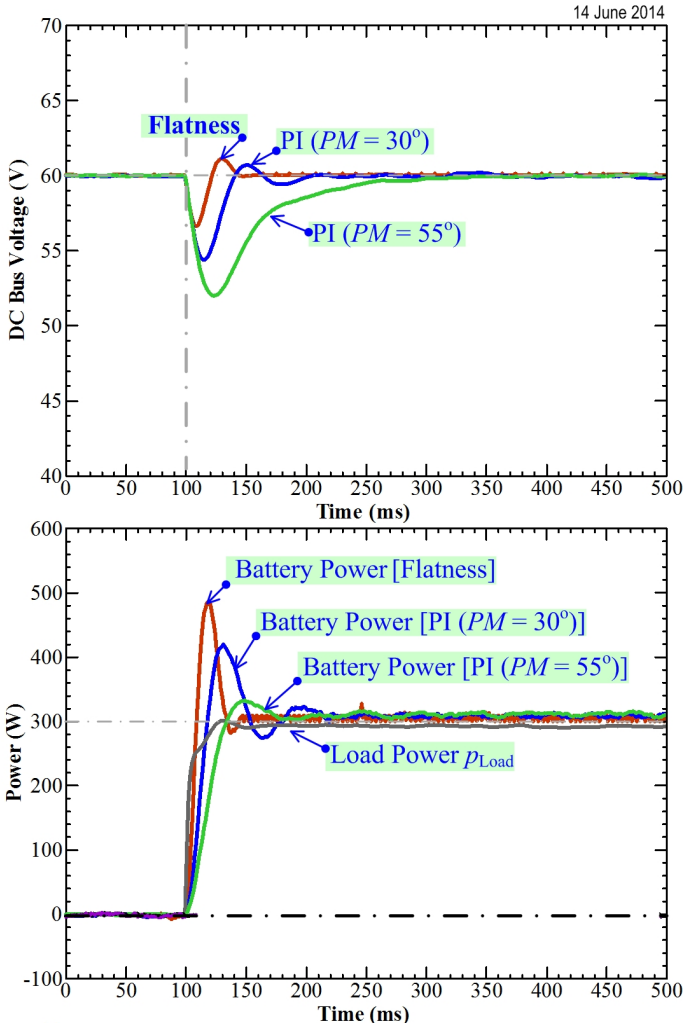

Fig. 3. Comparative study of the differential flatness-based control with a PI compensator by a Li-Ion battery connected with multi-phase boost converters during an external load step from 0 W to 300 W at t = 100 ms [25].

The article is composed of four sections. After presenting the current literature on this research topic and the reasons to carry out this work; in section II, a short brief of the differential flatness based-control theory, a general description of the system, the differential equations of the complex FC converters, and the proposed control algorithm and stability proof are provided. Section III presents the validation of the proposed control algorithm through simulation and real test bench results in the laboratory. Lastly, conclusions and perspectives are given in Section IV.

II. DESIGN OF THE CONTROLLER

A. Summary of The Differential Flatness Control Approach

Firstly, before utilizing the differential flatness calculation approach, it is important to confirm that the system is flat. Flatness estimation was originally proposed by Fliess *et al*. [33] in 1995. Acknowledge the following nonlinear network:

$$\dot{\mathbf{x}} = f_1(\mathbf{x},\mathbf{u}), \quad \mathbf{x} \in \Re^{\mathrm{n}}, \mathbf{u} \in \Re^{\mathrm{m}} \tag{1}$$

$$\mathbf{y} = f_2(\mathbf{x},\mathbf{u}), \quad \mathbf{y} \in \Re^{\mathrm{m}} \tag{2}$$

where **y** is output vector (here, named the *flat outputs*), **x** is state variables (or state vector), and **u** is input or control variables.

Mathematically, a nonlinear network can be determined as a flatness when the following two essential constraints are fulfilled:

1) The flat outputs **y** can be presented in the function of control input variables **u**, state vector **x** and a finite number of input's derivatives

$$\mathbf{y} = f_{\mathrm{y}}\left(x,u,\dot{u},\ddot{u},\ldots u^{(\alpha)}\right) \tag{3}$$

2) The state vector **x** and control input variables **u** can be written according to the flat outputs **y** and a finite number of its derivatives as

$$\mathbf{x} = f_{\mathrm{x}}\left(y,\dot{y},\ddot{y}\ldots.y^{(\beta)}\right) \tag{4}$$

$$\mathbf{u} = f_{\mathrm{u}}\left(y,\dot{y},\ddot{y}\ldots.y^{(\gamma)}\right) \tag{5}$$

where α, β, and γ are positive integers; these numbers depend on the order of the system and $\mathbf{y}^{(r)}$ is the rth derivative for time. The flat output variables **y** are equal in number to the control vector **u**.

If the selected output variables can be verified to be flat output variables ***y***, the desired output reference $\mathbf{y}_{\mathrm{d}}$ becomes uncomplicated and straightforward. Indeed, for the 1st order ordinary differential equations, the dynamics of the appearing error dynamics can be defined by providing a new stabilizing output λ (named here, "control law", as shown in Fig. 4) [34],[35].

$$0 = \left(\ddot{y} - \ddot{y}_{\mathrm{d}}\right) + K_{\mathrm{p}}\left(\dot{y} - \dot{y}_{\mathrm{d}}\right) + K_{\mathrm{i}}\left(y - y_{\mathrm{d}}\right). \tag{6}$$

Then,

$$\lambda = \dot{y} = \dot{y}_{\mathrm{d}} + K_{\mathrm{p}}\left(y_{\mathrm{d}} - y\ \right) + K_{\mathrm{i}}\int\left(y_{\mathrm{d}} - y\right)d\tau \tag{7}$$

where K_{p} and K_{i} are the set of controller parameters. According to (5) and (7), for the 1st order ordinary differential equations, these results in the following control vector:

$$\mathbf{u} = f_{\mathrm{u}}\left(y, \lambda\right) \tag{8}$$

where the control variables are estimated depending on the desired flat outputs $\mathbf{y}_{\mathrm{d}}$ and measured flat outputs $\mathbf{y}$. The controller parameters K_{p} and K_{i} are chosen such that the roots of the second-order standard equation, in the complex variable s [36],

$$\frac{y(s)}{y_{\mathrm{d}}(s)} = \frac{{\omega_{\mathrm{n0}}}^2}{\mathrm{s}^2 + 2\zeta_0\omega_{\mathrm{n0}}\mathrm{s} + {\omega_{\mathrm{n0}}}^2} \tag{9}$$

Evidently, the error signal, $e = y - y_{\mathrm{d}}$, yields

$$\ddot{e} + K_{\mathrm{p}}\dot{e} + K_{\mathrm{i}}e = \mathrm{s}^2 + 2\zeta_0\omega_{\mathrm{n0}}\mathrm{s} + {\omega_{\mathrm{n0}}}^2 . \tag{10}$$

$$K_{\mathrm{p}} = 2\zeta_0\omega_{\mathrm{n0}}, \quad K_{\mathrm{i}} = {\omega_{\mathrm{n0}}}^2 . \tag{11}$$

where, ζ_0 and ω_{n0} are the standard 2nd order damping ratio and natural frequency that specify properties such as response time, overshoot, and bandwidth. Note here that equation (9) is written in the complex frequency domain; however, it is simple in time domain representation as shown in Fig. 4, and to implement in a microcontroller by coding a software programming (Simulink Blocks; C or Assembly languages), it is composed of 3 terms: proportional, integral, and derivative terms.

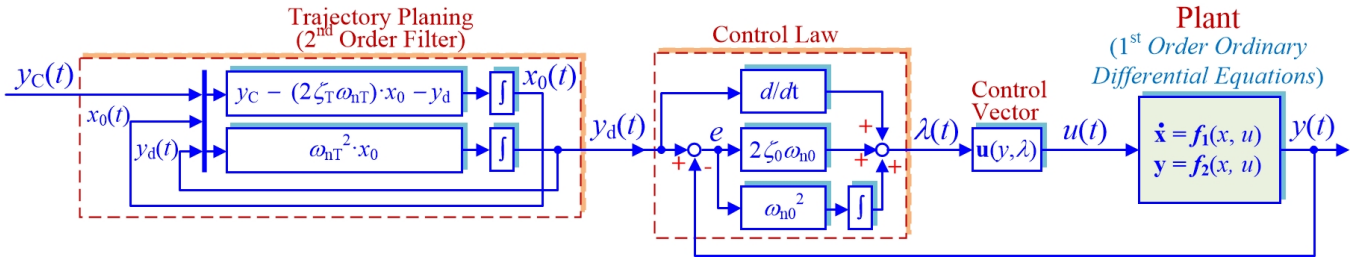

Fig. 4. Concept of the differential flatness control approach of the 1st order ordinary differential equations.

Finally, the trajectory of y_{d} is defined to determine the following requirements: response time of the flat output variable y and limiting the maximum power during the initial state. For this reason, the trajectory response of y_{d} is formed to be a 2nd order system by using a standard 2nd order equation as follows [37]:

$$\frac{y_{\mathrm{d}}(s)}{y_{\mathrm{C}}(s)} = \frac{{\omega_{\mathrm{nT}}}^2}{\mathrm{s}^2 + 2\zeta_{\mathrm{T}}\omega_{\mathrm{nT}}\mathrm{s} + {\omega_{\mathrm{nT}}}^2} \tag{12}$$

where, y_{C} is the command signal, ζ_1 and ω_{n1} are the defined damping ratio and natural frequency. It is displayed in Fig. 4 and should be noted that x_0 is the internal state variable in time domain.

B. Multistack FC with Multiphase Parallel Boost Converter Modeling

Fig. 2 shows the circuits of the studied DC/DC power converters for FC higher power applications. To simplify, the two FC stacks and two-phase parallel interleaved boost converters for each stack are studied. The well-known port-Hamiltonian form of the boost converters are written as [38] – [40]:

$$\frac{d\mathbf{x}}{dt} = [\mathbf{J}(x) - \mathbf{R}(x)] \cdot \frac{\partial \mathbf{H}(x)}{\partial x} + \mathbf{g}(x) \cdot \mathbf{u} + \boldsymbol{\xi}, \tag{13}$$

where $\mathbf{x} \in \Re^n$ is the state vector; $\mathbf{u} \in \Re^m$ is the input control vector; $\mathbf{H}$ is the global stored energy; $\mathbf{J}$ and $\mathbf{R}$ are the natural interconnection and damping matrices, respectively, with $\mathbf{J} = -\mathbf{J}^{\mathrm{T}}$ and $\mathbf{R} = \mathbf{R}^{\mathrm{T}} \geq 0$; $\mathbf{g}$ is the port characteristic matrix; and $\boldsymbol{\xi}$ is the external disturbance vector. Then, one writes:

$$\overbrace{\begin{bmatrix} \frac{di_{\mathrm{L11}}}{dt} \\ \frac{di_{\mathrm{L12}}}{dt} \\ \frac{di_{\mathrm{L21}}}{dt} \\ \frac{di_{\mathrm{L22}}}{dt} \\ \frac{dv_{\mathrm{C}}}{dt} \end{bmatrix}}^{\mathrm{d}\mathbf{x}/\mathrm{d}t} = \overbrace{\begin{bmatrix} -\frac{r_{\mathrm{L11}}}{L_{11}^2} & 0 & 0 & 0 & -\frac{1}{L_{11}C_{\mathrm{B}}} \\ 0 & -\frac{r_{\mathrm{L12}}}{L_{12}^2} & 0 & 0 & -\frac{1}{L_{12}C_{\mathrm{B}}} \\ 0 & 0 & -\frac{r_{\mathrm{L21}}}{L_{21}^2} & 0 & -\frac{1}{L_{21}C_{\mathrm{B}}} \\ 0 & 0 & 0 & -\frac{r_{\mathrm{L22}}}{L_{22}^2} & -\frac{1}{L_{22}C_{\mathrm{B}}} \\ \frac{1}{L_{11}C_{\mathrm{B}}} & \frac{1}{L_{12}C_{\mathrm{B}}} & \frac{1}{L_{21}C_{\mathrm{B}}} & \frac{1}{L_{22}C_{\mathrm{B}}} & 0 \end{bmatrix}}^{\mathbf{J}(x)-\mathbf{R}(x)} \overbrace{\begin{bmatrix} L_{11}i_{\mathrm{L11}} \\ L_{12}i_{\mathrm{L12}} \\ L_{21}i_{\mathrm{L21}} \\ L_{22}i_{\mathrm{L22}} \\ C_{\mathrm{B}}v_{\mathrm{C}} \end{bmatrix}}^{\partial \mathbf{H}(x)/\partial \mathbf{x}} + \overbrace{\begin{bmatrix} \frac{v_{\mathrm{C}}}{L_{11}} & 0 & 0 & 0 \\ 0 & \frac{v_{\mathrm{C}}}{L_{12}} & 0 & 0 \\ 0 & 0 & \frac{v_{\mathrm{C}}}{L_{21}} & 0 \\ 0 & 0 & 0 & \frac{v_{\mathrm{C}}}{L_{22}} \\ -\frac{i_{\mathrm{L11}}}{C_{\mathrm{B}}} & -\frac{i_{\mathrm{L12}}}{C_{\mathrm{B}}} & -\frac{i_{\mathrm{L21}}}{C_{\mathrm{B}}} & -\frac{i_{\mathrm{L22}}}{C_{\mathrm{B}}} \end{bmatrix}}^{\mathbf{g}(x)} \overbrace{\begin{bmatrix} d_{11} \\ d_{12} \\ d_{21} \\ d_{22} \end{bmatrix}}^{\mathbf{u}} + \overbrace{\begin{bmatrix} \frac{v_{\mathrm{FC1}}}{L_{11}} \\ \frac{v_{\mathrm{FC1}}}{L_{12}} \\ \frac{v_{\mathrm{FC2}}}{L_{21}} \\ \frac{v_{\mathrm{FC2}}}{L_{22}} \\ \frac{-i_{\mathrm{Load}}}{C_{\mathrm{B}}} \end{bmatrix}}^{\boldsymbol{\xi}}, \tag{14.1}$$

$$\text{with, } \mathbf{H}(x) = \frac{1}{2}\left(L_{11}i_{\mathrm{L11}}^2 + L_{12}i_{\mathrm{L12}}^2 + L_{21}i_{\mathrm{L21}}^2 + L_{22}i_{\mathrm{L22}}^2 + C_{\mathrm{B}}v_{\mathrm{C}}^2\right), \tag{14.2}$$

where d is the controlled duty cycles of the converter ($d \in [0,1]$), , v_{C} is the DC bus voltage, i_{L} is the inductor current, i_{Load} is the external load current at the DC bus, C_{B} is the DC bus capacitance, L is the input inductance of both interleaved boost converters, r_{L} represents the losses in each DC/DC converter module, v_{FC1} and v_{FC2} are the FC voltages of the first and second stacks, i_{FC1} (= i_{L11} + i_{L12}) is the first FC current, and finally i_{FC2} (= i_{L21} + i_{L22}) is the second FC current.

The stored energy E_{B} in the DC bus capacitance C_{B} can be expressed as follows:

$$E_{\mathrm{B}} = \frac{1}{2}C_{\mathrm{B}}{v_{\mathrm{C}}}^2 \tag{15}$$

A reduced-order model of the studied FC boost power converters is illustrated in Fig. 5. The derivative of the DC bus stored energy E_{B} according to p_{FC1o}, p_{FC1o}, and p_{Load} is given by:

$$\dot{E}_{\mathrm{B}} = \overbrace{\overbrace{p_{11\mathrm{o}} + p_{12\mathrm{o}}}^{p_{\mathrm{FC1o}}} + \overbrace{p_{21\mathrm{o}} + p_{22\mathrm{o}}}^{p_{\mathrm{FC2o}}}}^{p_{\mathrm{T}}} - p_{\mathrm{Load}} \tag{16}$$

where,

$$p_{11o} = v_{FC1} \cdot i_{L11} - r_{L11} \cdot {i_{L11}}^2 \tag{17.1}$$

$$p_{12o} = v_{FC1} \cdot i_{L12} - r_{L12} \cdot {i_{L12}}^2 \tag{17.2}$$

$$p_{21o} = v_{FC2} \cdot i_{L21} - r_{L21} \cdot {i_{L21}}^2 \tag{17.3}$$

$$p_{22o} = v_{FC2} \cdot i_{L22} - r_{L22} \cdot {i_{L22}}^2 \tag{17.4}$$

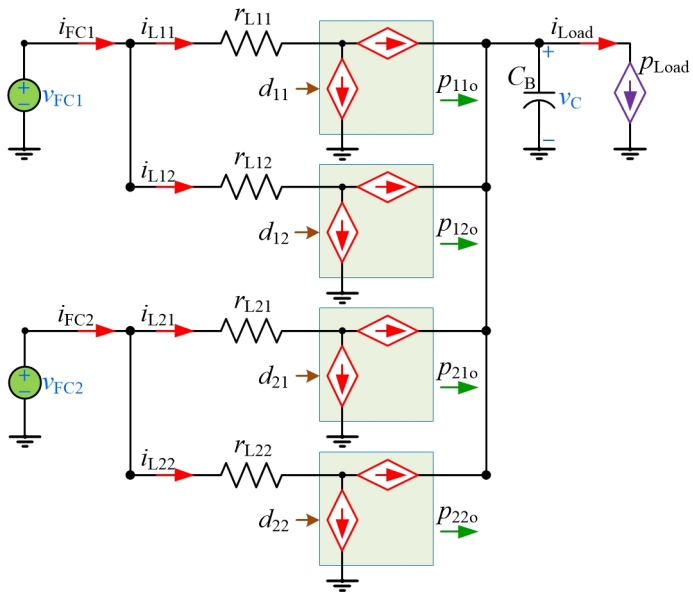

Fig. 5. Reduced-order model of the studied FC step-up power converters.

C. Inner Inductor Current Control

The FC powers p_{FC1} and p_{FC2} are determined as the output components. In this case, the total FC power is controlled through the FC current. At this point, 2-phase parallel DC/DC converters are implemented for each FC stack. In that case, one may express:

$$i_{FC1} = \frac{p_{FC1}}{v_{FC1}}, \; i_{FC2} = \frac{p_{FC2}}{v_{FC2}} \tag{18}$$

$$i_{L11} = i_{L12} = \frac{i_{FC1}}{2}, \; i_{L21} = i_{L22} = \frac{i_{FC2}}{2} \tag{19}$$

To prove that the current loop is flat, it has been decided to choose the inductor current as of the flat variables $\mathbf{y}_C = [i_{L11}, i_{L12}, i_{L21}, i_{L22}]^T$, and the control variables $\mathbf{u}_I = [d_{11}, d_{12}, d_{21}, d_{22}]^T$, afterward the state variables $\mathbf{x}_C$ can be written (refer to (4)) as

$$\begin{aligned} \mathbf{x}_I &= [i_{L11}, i_{L12}, i_{L21}, i_{L22}]^T \\ &= \mathbf{y}_I = f_{xI}(\mathbf{y}) \end{aligned} \tag{20}$$

Proof: According to (5) for the 1st order system $\mathbf{u} = f_u(y, \dot{y})$ and (13.1) – (13.4), the control vector $\mathbf{u}_C$ can be derived as follows:

$$\mathbf{u}_{\mathrm{I}}=\begin{bmatrix} d_{11} \\ d_{12} \\ d_{21} \\ d_{22} \end{bmatrix}=\begin{bmatrix} 1-v_{\mathrm{FC1}}/v_{\mathrm{C}} \\ 1-v_{\mathrm{FC1}}/v_{\mathrm{C}} \\ 1-v_{\mathrm{FC2}}/v_{\mathrm{C}} \\ 1-v_{\mathrm{FC2}}/v_{\mathrm{C}} \end{bmatrix}+\begin{bmatrix} r_{\mathrm{L11}}/v_{\mathrm{C}} & 0 & 0 & 0 \\ 0 & r_{\mathrm{L12}}/v_{\mathrm{C}} & 0 & 0 \\ 0 & 0 & r_{\mathrm{L21}}/v_{\mathrm{C}} & 0 \\ 0 & 0 & 0 & r_{\mathrm{L22}}/v_{\mathrm{C}} \end{bmatrix}\cdot\mathbf{y}_{\mathrm{I}}+\begin{bmatrix} \mathrm{L}_{11}/v_{\mathrm{C}} & 0 & 0 & 0 \\ 0 & \mathrm{L}_{12}/v_{\mathrm{C}} & 0 & 0 \\ 0 & 0 & \mathrm{L}_{21}/v_{\mathrm{C}} & 0 \\ 0 & 0 & 0 & \mathrm{L}_{22}/v_{\mathrm{C}} \end{bmatrix}\cdot\dot{\mathbf{y}}_{\mathrm{I}} \quad (21)$$
$$=f_{\mathrm{uC}}(\mathbf{y}_{\mathrm{I}},\dot{\mathbf{y}}_{\mathrm{I}})$$

According to the flatness control theory presented in the subsection A, it is obvious that the current loops can be proved as a flat system because (20) and (21) are reliable with (4) and (5).

Finally, refer to (7), (10), and (11), the feedback control law is set:

$$\boldsymbol{\lambda}_{\mathrm{I}}=\dot{\mathbf{y}}_{\mathrm{Id}}+K_{\mathrm{pI}}(\mathbf{y}_{\mathrm{Id}}-\mathbf{y}_{\mathrm{I}})+K_{\mathrm{iI}}\int_0^t(\mathbf{y}_{\mathrm{Id}}-\mathbf{y}_{\mathrm{I}})d\tau \quad (22)$$

where $\mathbf{K}_{\mathrm{pI}}=diag\{K_{\mathrm{pI11}},K_{\mathrm{pI12}},K_{\mathrm{pI21}},K_{\mathrm{pI22}}\}$ and $\mathbf{K}_{\mathrm{iI}}=diag\{K_{\mathrm{iI11}},K_{\mathrm{iI12}},K_{\mathrm{iI21}},K_{\mathrm{iI22}}\}$ and

$$\mathbf{K}_{\mathrm{pI}}=2\zeta_{\mathrm{I}}\omega_{\mathrm{nI}},\quad \mathbf{K}_{\mathrm{iI}}=\omega_{\mathrm{nI}}{}^2. \quad (23)$$

Finally, according to (12), the trajectory response of $\mathbf{y}_{\mathrm{Id}}$ is set as follows:

$$\frac{\mathbf{y}_{\mathrm{Id}}(s)}{\mathbf{y}_{\mathrm{IC}}(s)}=\frac{\omega_{\mathrm{nTI}}{}^2}{\mathrm{s}^2+2\zeta_{\mathrm{TI}}\omega_{\mathrm{nTI}}\mathrm{s}+\omega_{\mathrm{nTI}}{}^2} \quad (24)$$

D. Outer DC Bus Voltage Control

To stabilize the DC bus voltage v_{C} to the desiderate value v_{Cd}, a flatness estimator has been employed. In this work, the DC bus voltage is indirectly regulated by stabilizing the stored energy in the output capacitance C_{B}. Therefore, it has been defined that the DC bus stored energy E_{B} (refer to (15) is the candidate flat variable y_{V}. Then, the state variable x_{V} can be estimated according to the flat variable:

$$x_{\mathrm{V}}=\sqrt{\frac{2y_{\mathrm{V}}}{\mathrm{C_B}}}=f_{\mathrm{xV}}(y) \quad (25)$$

Proof: According to (5) for the 1st order system $\mathbf{u}=f_{\mathrm{u}}(y,\dot{y})$ and (16), the control variable $\mathbf{u}_{\mathrm{V}}$ can be derived as follows:

$$u_{\mathrm{V}}=P_{\mathrm{T}}=\dot{y}_{\mathrm{V}}+\sqrt{\frac{2y_{\mathrm{V}}}{\mathrm{C_B}}}\cdot i_{\mathrm{Load}} \quad (26)$$
$$=f_{\mathrm{uV}}(\mathbf{y}_{\mathrm{V}},\dot{\mathbf{y}}_{\mathrm{V}})$$

According to the flatness control theory presented in section A, the outer energy control loop can be proved as a flat system because (25) and (26) are reliable with (4) and (5).

Again, refer to (7), (10), and (11), the closed-loop control law is set:

$$\boldsymbol{\lambda}_{\mathrm{V}}=\dot{y}_{\mathrm{V}}=\dot{y}_{\mathrm{Vd}}+K_{\mathrm{pV}}(y_{\mathrm{Vd}}-y_{\mathrm{V}})+K_{\mathrm{iV}}\int_0^t(y_{\mathrm{Vd}}-y_{\mathrm{V}})d\tau \quad (27)$$

where

$$K_{\mathrm{pV}}=2\zeta_{\mathrm{V}}\omega_{\mathrm{nV}},\quad K_{\mathrm{iV}}=\omega_{\mathrm{nV}}{}^2 \quad (28)$$

Finally, according to (12), the trajectory response of y_{Vd} is set as follows:

$$\frac{y_{Vd}(s)}{y_{VC}(s)} = \frac{{\omega_{nTV}}^2}{s^2 + 2\zeta_{TV}\omega_{nTV}s + {\omega_{nTV}}^2} \tag{29}$$

E. Summary of the Control Laws and Stability Analysis

The proposed control of the FC power plant previously introduced is displayed in Fig. 6. A DC bus voltage reference v_{Cd} and a DC bus voltage measurement v_C are transformed to energy signals y_{VC} and y_V by using (15). Then, the energy trajectory planning (29) generates an energy set-point y_{Vd}. Next, the control law (28) and the control vector (27) generates an FC total power reference p_T (= u_V); this signal is restricted to protect the total FC power within an interval [minimum power P_{TMin}, maximum power P_{TMax}]. This results in the FC stack powers (with limitation within an interval [P_{FC1Min}, P_{FC1Max}] and [P_{FC2Min}, P_{FC2Max}]) and the converter powers as follows:

$$p_{FC1o} = p_{FC2o} = p_T/2 \tag{30.1}$$

$$p_{11o} = p_{12o} = p_{FC1o}/2\,,\ p_{21o} = p_{22o} = p_{FC2o}/2 \tag{30.2}$$

According to (17), the inductor current commands $\mathbf{y}_{IC} = [i_{L11C}, i_{L12C}, i_{L21C}, i_{L22C}]^T$ can be expressed as follows:

$$i_{L11C} = i_{L12C} = 2\frac{p_{1Max}}{v_{FC1}}\left(1 - \sqrt{1 - p_{11o}/p_{1Max}}\right)\Big|_{r_{L11}=r_{L12}} \tag{30.3}$$

$$i_{L21C} = i_{L22C} = 2\frac{p_{1Max}}{v_{FC2}}\left(1 - \sqrt{1 - p_{21o}/p_{2Max}}\right)\Big|_{r_{L21}=r_{L22}} \tag{30.4}$$

with,

$$p_{1Max} = \frac{v_{FC1}^2}{4r_{L11}}\,,\ p_{2Max} = \frac{v_{FC2}^2}{4r_{L21}} \tag{30.5}$$

For safety reasons, the inductor current command i_{LC} (= $\mathbf{y}_{IC}$) has to be set in rank, i.e., within a space [minimum current I_{LMin} (set to 0 A), maximum current I_{LMax} (corresponding to a converter rated power)]. Afterward, the trajectory planning (24) estimates an inductor current demand y_{Id}. As a final point, the control laws (22) and control vector (21) generate duty cycle control signals $\mathbf{u}_I = [d_{11}, d_{12}, d_{21}, d_{22}]^T$.

Stability Proof: The association between and the high switching frequency f_S and the above-mentioned natural frequency ω_n is roughly particular based on the cascade control structure [41]. According to the *Nyquist* theorem, the desired natural frequency can be expressed as follows:

$$\omega_{nTV} << \omega_{nV} << \omega_{nTI} << \omega_{nI} << 2\cdot\pi\cdot f_S\ (= \omega_S). \tag{31}$$

According to the *Symmetrical Optimum Method*, the desired damping coefficient ζ can be tuned as follows:

$$\zeta_V = \zeta_I = \frac{1}{\sqrt{2}}\Big|_{\text{Control Laws}}\,,\ \zeta_{TV} = \zeta_{TI} = 1\Big|_{\text{Trajectory Planing}}. \tag{32}$$

Finally, the proposed flatness control approach is a nonlinear model-based control, in which the system needs to know the system parameters (C_B, r_L, L) referred as the control vector (21), the current command

generations (30), and the energy generation (15). This is the main disadvantage of this control algorithm. However, model errors and system uncertainties, the integral actions of the flat outputs (y_V and y_I) are introduced to the closed-loop system. This integral term [linked to the integral gains K_{iI} (22) and K_{iV} (27)] excellently compensates the system uncertainties such as the uncertainties in r_L, L, etc., so that it can guarantee that the flat output set-point y_d is always equal to the flat output y at the equilibrium point.

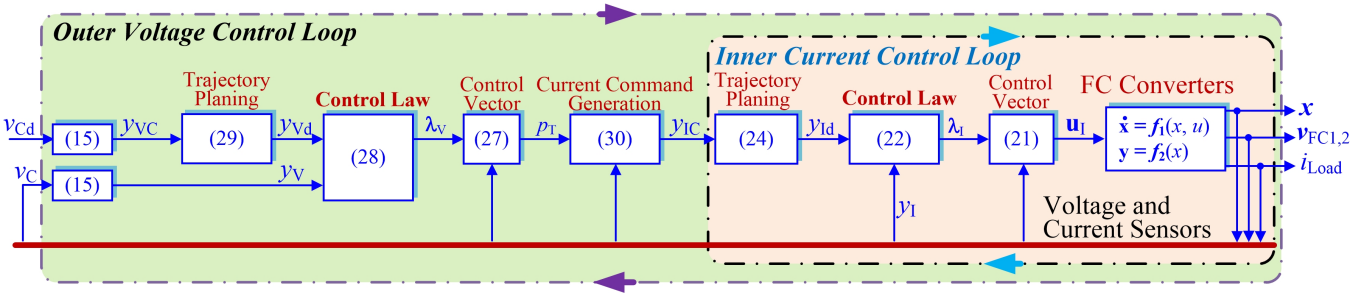

Fig. 6. Designed cascade control loop scheme for multi-stack FC with multiphase interleaved boost converters.

III. Performance Validation

The FC/hydrogen reformer system and FC converter test bench are realized to substantiate the performance of the proposed control approach, as illustrated in Fig. 7. The tested FC reformer engine includes a ME²Power Fuel Cell System: stack #1 2.5 kW, 50 V, and stack #2 2.5 kW, 50 V. The 5 kW Methanol System (2.5 kW for each stack) consists of using a fuel reformer reactor that converts chemically methanol fuel with water into hydrogen H_2 to both FC stacks. The proposed controller algorithm (see Fig. 6) is realized through a dSPACE MicroLabBox platform linking the mathematical estimations of MATLAB–Simulink with a sampling frequency of 25 kHz (= 40 μs of the sampling time) (which is synchronized with a switching frequency f_S (= 25 kHz) of the FC converters). The circuit parameters of the FC converters are summarized in Table I and the system control parameters are listed in Table II.

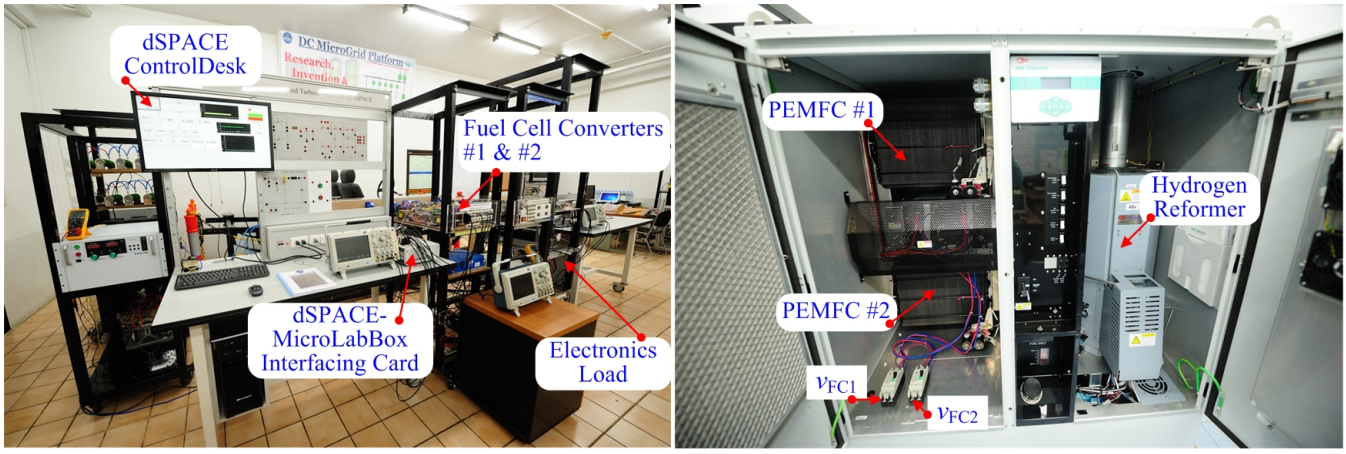

Fig. 7. Test bench platform of FC power plant supplied by 2-Stack PEMFCs/Reformer at the Renewable Energy Research Centre (RERC).

TABLE I. POWER BOOST CONVERTERS

Symbol	Quantity	Nominal Value
v_C	Nominal DC Bus Voltage	100 V
$v_{FC1} = v_{FC2}$	Nominal FC Voltage	50 V
$L_1 = L_2 = L_3 = L_4$	Inductances	200 μH
$r_{L11} = r_{L12} = r_{L21} = r_{L22}$	Resistive losses	0.06 Ω
C_B	DC bus capacitance	2,000 μF
f_S	Constant Switching Frequency	25 kHz
S_{11}, S_{12}, S_{21}, S_{22}	Power MOSFET, IXFN90N85X	850 V, 90 A

TABLE II. CONTROLLER PARAMETERS

Symbol	Value	Symbol	Value
ω_S	157,079 rad/s	P_{TMax}	5 kW
ω_{nI}	7,500 rad/s	P_{TMin}	0 kW
ω_{nTI}	750 rad/s	P_{FC1Max}	2.5 kW
ω_{nV}	75 rad/s	P_{FC2Max}	2.5 kW
ω_{nTV}	7.5 rad/s	P_{FC1Min}	0 kW
$\zeta_I = \zeta_V$	0.707 pu.	P_{FC2Min}	0 kW
$\zeta_{TV} = \zeta_{TI}$	1 pu.	I_{LMax}	25 A
		I_{LMin}	0 A

The screen waveforms in Figs. 8 and 9 display the switching behaviors of the parallel boost converters at the FC power of 700 W of the 1st FC converter and 780 W of the 2nd FC converter, respectively. In Fig. 8, CH1 is the measured inductor current i_{L11}, CH2 is the measured inductor current i_{L12}, CH3 is the FC current i_{FC1}, CH4 is the FC voltage v_{FC1}. In Fig. 9, CH1 is the measured inductor current i_{L21}, CH2 is measured the inductor current i_{L22}, CH3 is the FC current i_{FC2}, CH4 is the FC voltage v_{FC2}. The oscilloscope plots illustrate the inductor ripple current cancellation. i_{FC1} represents the sum of inductor currents i_{L11} and i_{L12}; while i_{FCs} is the sum of inductor currents i_{L21} and i_{L22}. The measurement current clamps were tuned at 5 A.div^{-1} ratios. Each FC converter is two-phase interleaved boost converters (Fig. 2) operating 180° out of phase; as a result, the inductor ripple currents contribute to compensate each other and decrease the FC ripple current generated by the input inductors. From these signals, one can be observed that the FC ripple currents are nearly zero.

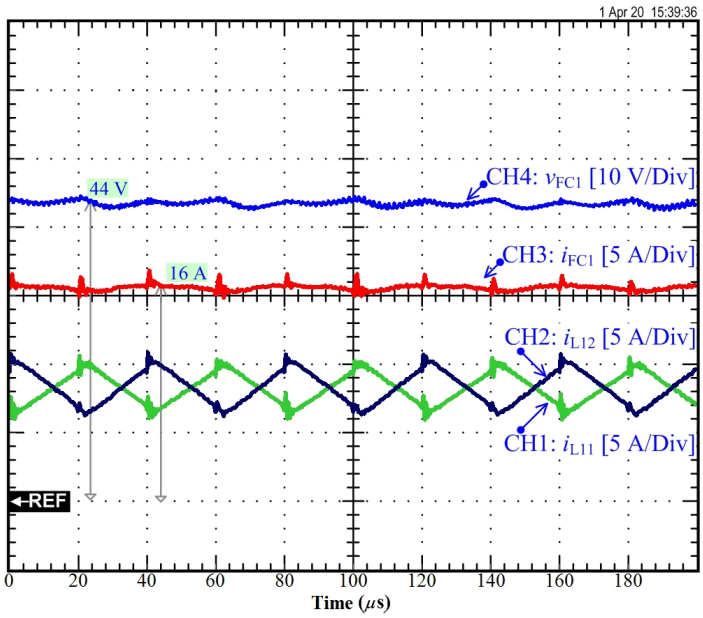

Fig. 8. Obtained experimental results: Switching waveforms of the 1st FC converter at p_{FC1} = 700 W.

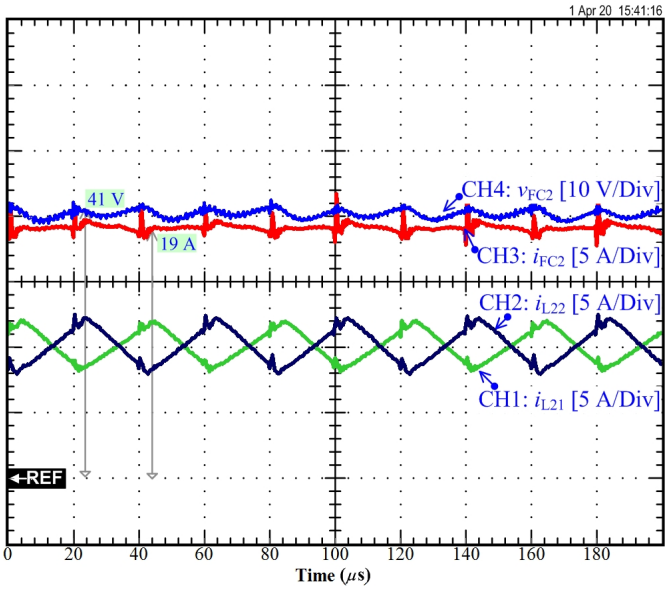

Fig. 9. Obtained experimental results: Switching waveforms of the 2nd FC converter at p_{FC2} = 780 W.

Next, to reveal dynamic control of the DC bus voltage at different load steps, the screen waveforms in Figs. 10 and 11 illustrate the DC bus voltage v_C behavior to the large load power requested (disturbance); whereas the DC bus of 100 V was loaded with a controlled electronic load. In Figs. 10 and 11, CH1 is the DC bus voltage v_C, CH2 is the 1st FC voltage v_{FC1}, CH3 is the 2nd FC voltage v_{FC2}, CH4 is the external load power p_{Load}, CH5 is the FC power p_{FC1}, CH6 is the FC power p_{FC2}, CH7 is the duty cycle d_{11}, CH8 is the 1st FC current i_{FC1}, CH9 is the measured inductor current i_{L11}. For the first scenario, the load power p_{Load} was changed from 480 to 900 W (↑ positive transition) at t = 50 ms. Second, the load power was considered from 900 to 480 W (↓ negative transition) at t = 50 ms.. As can be observed in Figs. 10 and 11, the first FC power p_{FC1} was well controlled and always equal to the second FC power p_{FC2}, and the DC bus output voltage and the inductor currents settle to theirs equilibrium points with good dynamic performance under the two regimes. Thanks to the integrator action in the proposed

control laws (22) and (27), there are no steady−state errors of the DC bus voltage at the fixed-point and the DC bus voltage is slightly affected by the great load step.

Fig. 12 shows the signals that were collected during the long load cycle, including the DC bus voltage v_C, the 1st voltage v_{FC1}, the external load power p_{Load}, the 1st FC power p_{FC1}, the 2nd FC power p_{FC2}, the 1st FC current i_{FC1}, the 2nd FC current i_{FC2}, and the measured inductor current i_{L21}. In the initial state, the load power is around 500 W; as a result, the first FC power and second FC power are 250 W to supply the energy for the load. At t_1, the demanded load power has increased from to 500 W to 1,200 W; again the first FC power and second FC power are 600 W. Next, at t_2, the requested load power has risen up from to 1,200 W to 500 W; at t_3, the load power steps from to 500 W to around 1,800 W; and finally at t_4, the load power has increased from to 1,800 W to 500 W. Once again, the first FC power p_{FC1} was well regulated and constantly equal to the second FC power p_{FC2} to supply the energy for the load ($p_{Load} \approx p_{FC1} + p_{FC2}$). The essential variable necessary to stabilize the energy in this complicated network is the DC bus voltage. From the laboratory tested corroboration, the DC bus voltage is intelligently regulated at the constant desired value, i.e., v_C = 100 V. This laboratory test authenticates that the energy in the DC microgrid is well managed.

For the sake of comparison, a conventional cascade linear PI control method is briefly explained. The inner control loops consist of four inductor currents i_{L11}, i_{L12}, i_{L21}, i_{L22}, and the outer control loop consists of dc-bus voltage v_C. The linear feedback PI control laws are given by the following expressions:

$$d_{11} = K_{Pi}\left(i_{L11d} - i_{L11}\right) + K_{Ii}\int_0^t \left(i_{L11d} - i_{L11}\right)d\tau\,, \tag{33.1}$$

$$d_{12} = K_{Pi}\left(i_{L12d} - i_{L12}\right) + K_{Ii}\int_0^t \left(i_{L12d} - i_{L12}\right)d\tau\,, \tag{33.2}$$

$$d_{21} = K_{Pi}\left(i_{L21d} - i_{L21}\right) + K_{Ii}\int_0^t \left(i_{L21d} - i_{L21}\right)d\tau\,, \tag{33.3}$$

$$d_{22} = K_{Pi}\left(i_{L22d} - i_{L22}\right) + K_{Ii}\int_0^t \left(i_{L22d} - i_{L22}\right)d\tau\,, \tag{33.3}$$

$$p_{FCd} = K_{Pv}\left(v_{Cd} - v_C\right) + K_{Iv}\int_0^t \left(v_{Cd} - v_C\right)d\tau\,, \tag{33.4}$$

$$\text{with, } p_{FC1d} = p_{FC2d} = \frac{p_{FCd}}{2}\,,\ i_{L11d} = i_{L21d} = \left(\frac{p_{FC1d}}{v_{FC1}}\right)\Big/2\,,\ i_{L21d} = i_{L22d} = \left(\frac{p_{FC2d}}{v_{FC2}}\right)\Big/2\,, \tag{33.5}$$

where K_{Pi}, K_{Ii}, K_{Pv}, and K_{Iv} are the set of controller parameters.

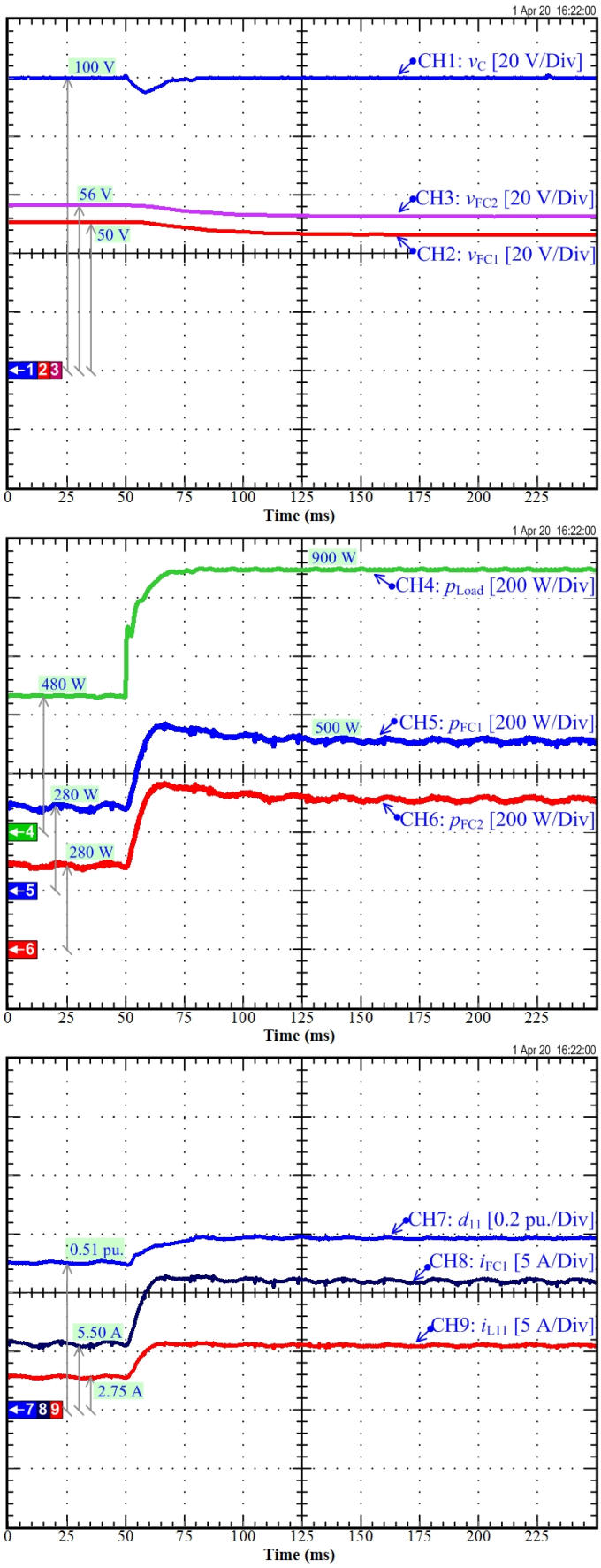

Fig. 10. Experimental results: Dynamic performance of the FC converter during a load power increase from 480 W to 900 W.

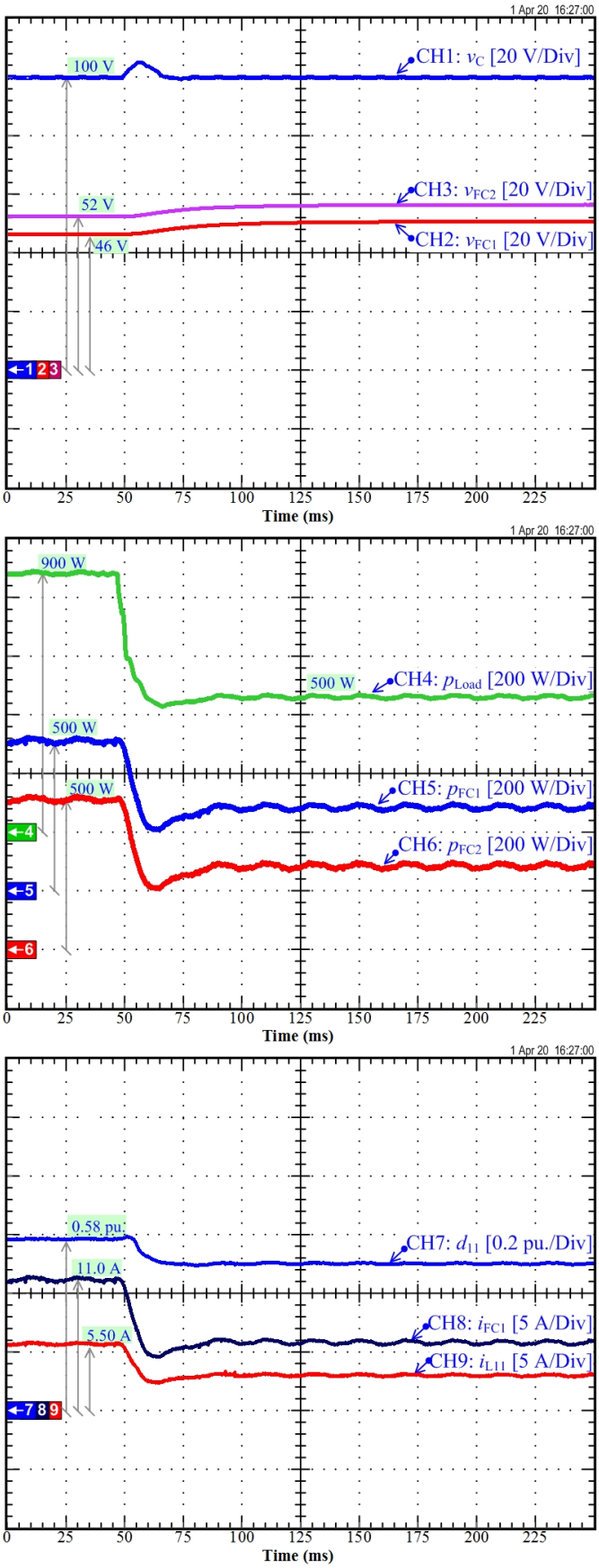

Fig. 11. Experimental results: Dynamic performance of the FC converter during a load power decrease from 900 W to 500 W.

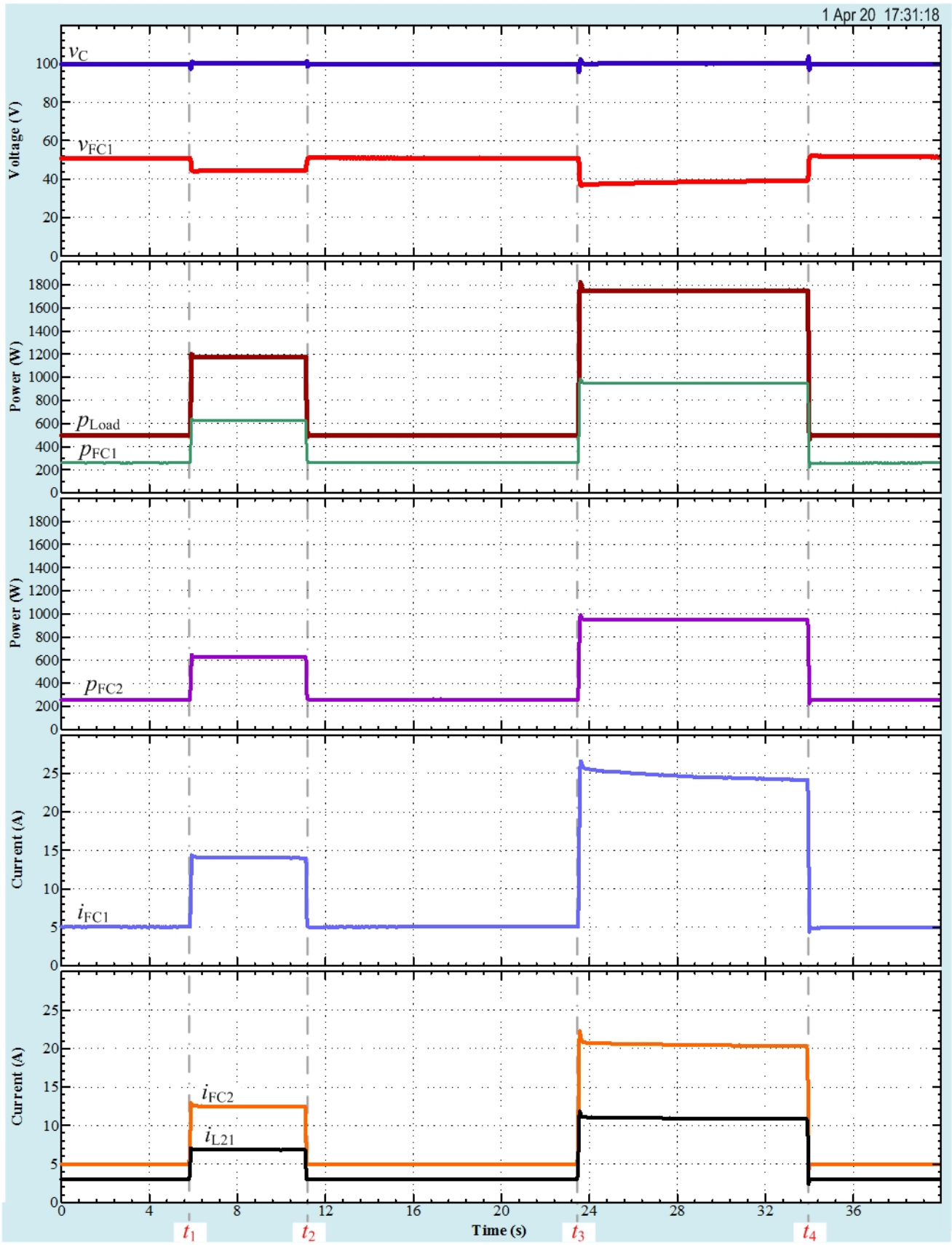

Fig. 12. Experimental results: FC converter response during load cycle.

To compare the effectiveness of the proposed flatness control laws and classic linear PI control laws, a numerical simulation has been performed. The simulations performed by MATLAB/Simulink are functioned using a switching model of the four-phase boost converters. To give a reasonable comparison between the methods, the parameters of the linear PI controllers have been tuned to obtain the best possible performance. Subsequently, K_{Pi} = 0.005 A^{-1}, K_{Ii1} = 400 $A \cdot s^{-1}$, K_{Pv} = 25 $W \cdot V^{-1}$, and K_{Iv} = 2,500 $W \cdot V \cdot s^{-1}$. Fig. 13 shows the simulation results obtained for both control laws during a large load step from 480 W to 900 W at t = 50 ms. CH1–CH8 represent the DC-bus voltage, first FC voltage, first FC current, load power, first-inductor current i_{L11}, fourth-inductor current i_{L22}, first duty cycle d_{11}, and fourth duty cycle d_{22}, respectively. The proposed flatness control laws exhibit good convergence of the dc-bus voltage regulation to its desired set-point of 100 V (= v_{Cd}). Although the dynamic response of the linear control law could be improved relative to that shown in Figure 13(a), this enhancement could come at the expense of a system oscillation. From these results, we conclude that the proposed flatness control provided better performance than the classical PI controller.

Finally, given that the proposed flatness control lives in the plane, it is possible to observe a global picture of the behavior of the controllers by drawing its phase plot (*vector field*): v_C VS i_{FC} ($i_{FC} = i_{FC1} + i_{FC2}$). This plot as shown in Fig. 14 is obtained by performing simulations of the closed–loop system with a wide range of initial conditions ( ): 600 W, 800 W, 1200 W, 1400 W, and 1600 W. It can be seen that the system converges to the desired equilibrium point [p_{Load} = 1000 W, $x_d = (i_{FCd}, v_{Cd})$ = (20.88 A, 100 V)].

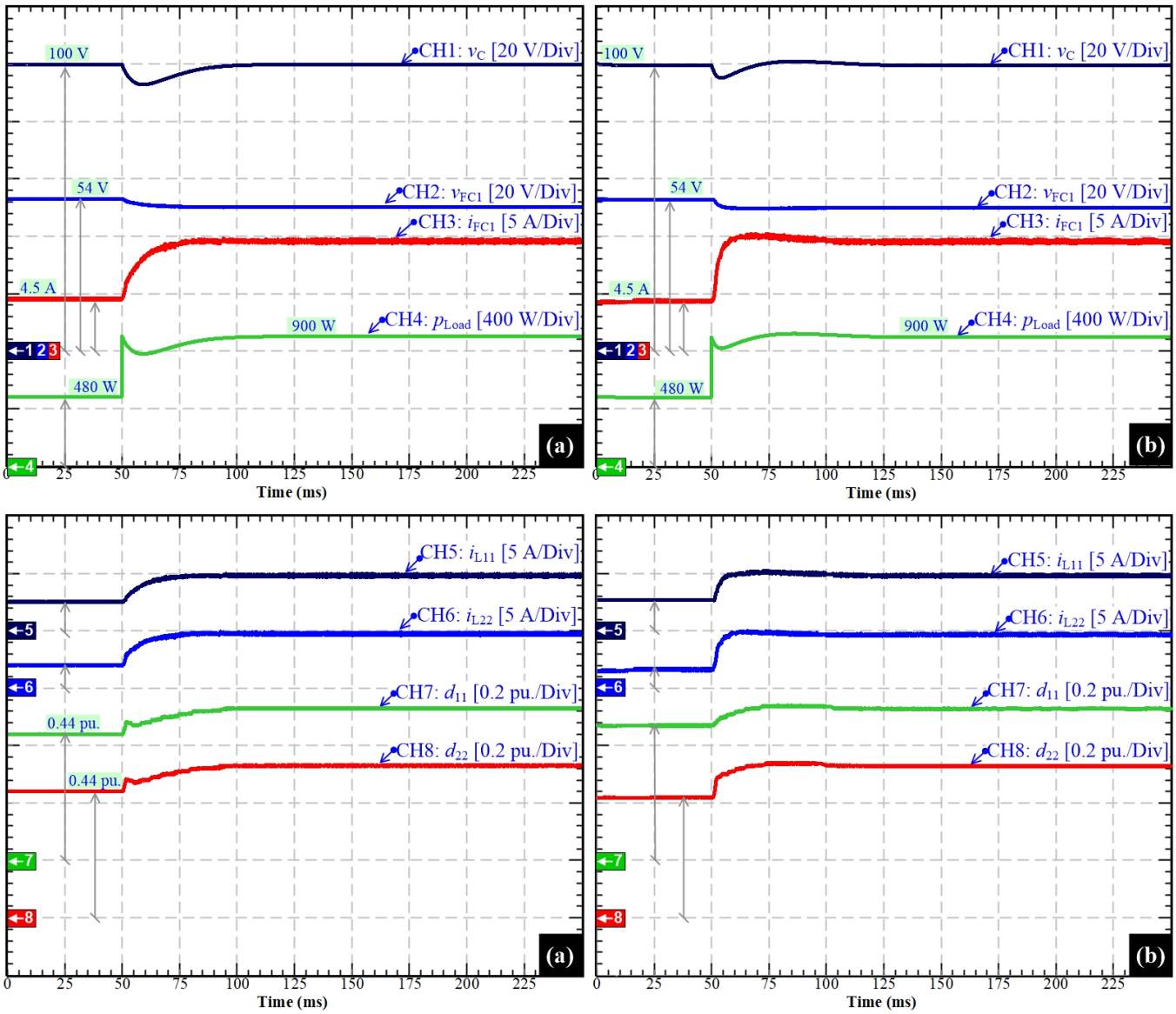

Fig. 13. Simulation results: Output voltage v_C regulation, contrasting the response of a PI controller against the proposed flatness controller: (a) cascade control based on PI controllers, (b) cascade control based on flatness controllers.

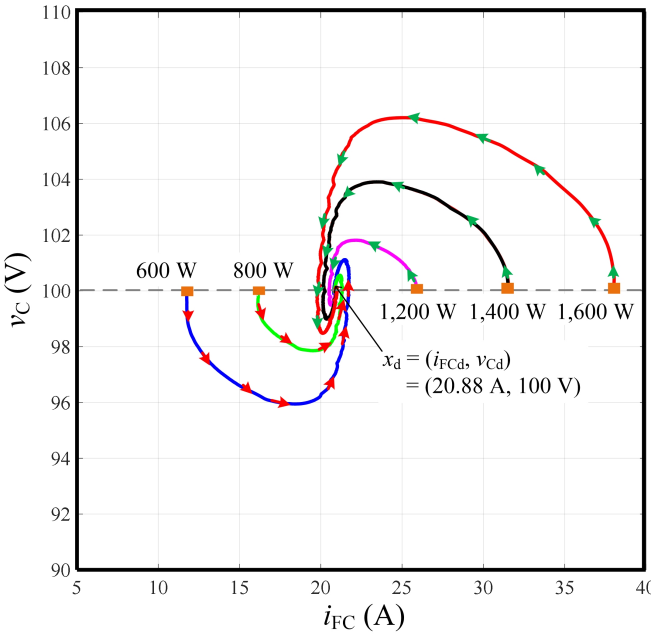

Fig. 14. Phase plots of the system with the proposed flatness control laws for different initial conditions.

IV. Conclusion

This article dealt with the investigation and design of nonlinear model-based control of a multi-stack PEMFC system with the multiphase interleaved boost converters. The multi-stack technology composes of several low powered fuel cell stacks in place of a single high powered fuel cell stack. A multi-stack FC system is attractive since it offers modularity, which makes the FC system substitution more suitable and fault-tolerant to ensure a continuity of service in case of electrical failures. A flatness-based control strategy has been applied to a multi-stack fuel cell system to ensure the stability of the DC bus and to manage the energy flows of both multi-stack fuel cells through their respective multiphase interleaved boost converters to face different dynamic load requests. The strategy is based on inner current loops applied to multiphase interleaved boost converters; whereas an outer voltage loop is applied to the DC bus for energy control. An experimental test including two PEMFC stacks (2.5 kW, 50 V) supplied by a hydrogen reformer (5 kW), and interleaved boost converters has been realized in the laboratory. The control algorithm has been implemented into a dSPACE MicroLabBox board and simulation in Matlab/Simulink. The obtained results both for steady-state and dynamic operations have enabled validating the excellent performance of the DC microgrid stabilization. In the continuity of this work, the DC microgrid will include an electrolyzer system (to take advantage of a long-term energy storage) to develop energy management based on nonlinear control to optimize the performance of the system.

Acknowledgment

This work was funded by the international research program in cooperation under Renewable Energy Research Centre (RERC) [King Mongkut's University of Technology North Bangkok (KMUTNB)] and Groupe de Recherche en Energie Electrique de Nancy (GREEN) [Université de Lorraine (UL)] under Grant KMUTNB–63–KNOW–040.

REFERENCES

[1] T. Lan, K. Strunz, Modeling of multi-physics transients in PEM fuel cells using equivalent circuits for consistent representation of electric, pneumatic, and thermal quantities, *International Journal Of Electrical Power & Energy Systems*. 119 (2020) 105803. doi:10.1016/j.ijepes.2019.105803.

[2] S. Mohiuddin, M. Mahmud, A. Haruni, H. Pota, Design and implementation of partial feedback linearizing controller for grid-connected fuel cell systems, International *Journal Of Electrical Power & Energy Systems*. 93 (2017) 414-425. doi:10.1016/j.ijepes.2017.06.015.

[3] N. Bizon, J. Lopez-Guede, E. Kurt, P. Thounthong, A. Mazare, L. Ionescu et al., Hydrogen economy of the fuel cell hybrid power system optimized by air flow control to mitigate the effect of the uncertainty about available renewable power and load dynamics, *Energy Conversion And Management*. 179 (2019) 152-165. doi:10.1016/j.enconman.2018.10.058.

[4] N. Bizon, G. Iana, E. Kurt, P. Thounthong, M. Oproescu, M. Culcer et al., Air Flow Real-time Optimization Strategy for Fuel Cell Hybrid Power Sources with Fuel Flow Based on Load-following, *Fuel Cells*. 18 (2018) 809-823. doi:10.1002/fuce.201700197.

[5] S. Collura, D. Guilbert, G. Vitale, M. Luna, F. Alonge, F. D'Ippolito et al., Design and experimental validation of a high voltage ratio DC/DC converter for proton exchange membrane electrolyzer applications, *International Journal Of Hydrogen Energy*. 44 (2019) 7059-7072. doi:10.1016/j.ijhydene.2019.01.210.

[6] T. Wang, Q. Li, Y. Qiu, L. Yin, L. Liu, W. Chen, Efficiency Extreme Point Tracking Strategy Based on FFRLS Online Identification for PEMFC System, *IEEE Transactions On Energy Conversion*. 34 (2019) 952-963. doi:10.1109/tec.2018.2872861.

[7] Y. Huangfu, Q. Li, L. Xu, R. Ma, F. Gao, Extended State Observer Based Flatness Control for Fuel Cell Output Series Interleaved Boost Converter, *IEEE Transactions On Industry Applications*. 55 (2019) 6427-6437. doi:10.1109/tia.2019.2936331.

[8] Y. Zhang, C. Zhang, Z. Huang, L. Xu, Z. Liu, M. Liu, Real-Time Energy Management Strategy for Fuel Cell Range Extender Vehicles Based on Nonlinear Control, *IEEE Transactions On Transportation Electrification*. 5 (2019) 1294-1305. doi:10.1109/tte.2019.2958038.

[9] A. Accetta, M. Pucci, Energy Management System in DC Micro-Grids of Smart Ships: Main Gen-Set Fuel Consumption Minimization and Fault Compensation, *IEEE Transactions On Industry Applications*. 55 (2019) 3097-3113. doi:10.1109/tia.2019.2896532.

[10] Q. Li, B. Su, Y. Pu, Y. Han, T. Wang, L. Yin et al., A State Machine Control Based on Equivalent Consumption Minimization for Fuel Cell/ Supercapacitor Hybrid Tramway, *IEEE Transactions On Transportation Electrification*. 5 (2019) 552-564. doi:10.1109/tte.2019.2915689.

[11] A. Kolli, A. Gaillard, A. De Bernardinis, O. Bethoux, D. Hissel, Z. Khatir, A review on DC/DC converter architectures for power fuel cell applications, Energy Conversion And Management. 105 (2015) 716-730. doi:10.1016/j.enconman.2015.07.060.

[12] M. Kabalo, B. Blunier, D. Bouquain, A. Miraoui, State-of-the-art of DC-DC converters for fuel cell vehicles, 2010 IEEE Vehicle Power And Propulsion Conference. (2010). doi:10.1109/vppc.2010.5729051.

[13] R. Ma, L. Xu, R. Xie, D. Zhao, Y. Huangfu, F. Gao, Advanced Robustness Control of DC–DC Converter for Proton Exchange Membrane Fuel Cell Applications, *IEEE Transactions On Industry Applications*. 55 (2019) 6389-6400. doi:10.1109/tia.2019.2935981.

[14] P. Mungporn, B. Yodwong, P. Thounthong, C. Ekkaravarodome, A. Bilsalam, B. Nahid-Mobarakeh et al., Study of Hamiltonian Energy Control of Multiphase Interleaved Fuel Cell Boost Converter, *2019 Research, Invention, And Innovation Congress (RI2C)*. (2019). doi:10.1109/ri2c48728.2019.8999956.

[15] P. Mungporn, B. Yodwong, P. Thounthong, B. Nahid-Mobarakeh, N. Takorabet, D. Guilbert et al., Model-Free Control of Multiphase Interleaved Boost Converter for Fuel Cell/Reformer Power Generation, *2019 Research, Invention, And Innovation Congress (RI2C)*. (2019). doi:10.1109/ri2c48728.2019.8999919.

[16] A. Macias Fernandez, M. Kandidayeni, L. Boulon, H. Chaoui, An Adaptive State Machine Based Energy Management Strategy for a Multi-Stack Fuel Cell Hybrid Electric Vehicle, *IEEE Transactions On Vehicular Technology*. 69 (2020) 220-234. doi:10.1109/tvt.2019.2950558.

[17] R. Umaz, A Single Inductor Self-Startup Energy Combiner Circuit with Bioturbation Resilience in Multiple Microbial Fuel Cells, *IEEE Transactions On Circuits And Systems II: Express Briefs*. (2020) 1-1. doi:10.1109/tcsii.2020.2972162.

[18] F. Sobrino-Manzanares, A. Garrigós, An interleaved, FPGA-controlled, multi-phase and multi-switch synchronous boost converter for fuel cell applications, International Journal Of Hydrogen Energy. 40 (2015) 12447-12456. doi:10.1016/j.ijhydene.2015.07.078.

[19] N. Marx, D. Hissel, F. Gustin, L. Boulon, K. Agbossou, On the sizing and energy management of an hybrid multistack fuel cell – Battery system for automotive applications, International Journal Of Hydrogen Energy. 42 (2017) 1518-1526. doi:10.1016/j.ijhydene.2016.06.111.

[20] M. Bahrami, J. Martin, G. Maranzana, S. Pierfederici, M. Weber, F. Meibody-Tabar et al., Multi-Stack Lifetime Improvement through Adapted Power Electronic Architecture in a Fuel Cell Hybrid System, Mathematics. 8 (2020) 739. doi:10.3390/math8050739.

[21] A. Macias, M. Kandidayeni, L. Boulon, H. Chaoui, A novel online energy management strategy for multi fuel cell systems, 2018 IEEE International Conference On Industrial Technology (ICIT). (2018). doi:10.1109/icit.2018.8352503.

[22] D. Dell'Isola, M. Urbain, M. Weber, S. Pierfederici, F. Meibody-Tabar, Optimal Design of a DC–DC Boost Converter in Load Transient Conditions, Including Control Strategy and Stability Constraint, *IEEE Transactions On Transportation Electrification*. 5 (2019) 1214-1224. doi:10.1109/tte.2019.2948038.

[23] S. Pang, B. Nahid-Mobarakeh, S. Pierfederici, M. Phattanasak, Y. Huangfu, G. Luo et al., Interconnection and Damping Assignment Passivity-Based Control Applied to On-Board DC–DC Power Converter System Supplying Constant Power Load, *IEEE Transactions On Industry Applications*. 55 (2019) 6476-6485. doi:10.1109/tia.2019.2938149.

[24] R. Gavagsaz-Ghoachani, M. Phattanasak, J. Martin, B. Nahid-Mobarakeh, S. Pierfederici, A Fixed-Frequency Optimization of PWM Current Controller—Modeling and Design of Control Parameters, *IEEE Transactions On Transportation Electrification*. 4 (2018) 671-683. doi:10.1109/tte.2018.2841801.

[25] Y. Huangfu, S. Zhuo, F. Chen, S. Pang, D. Zhao, F. Gao, Robust Voltage Control of Floating Interleaved Boost Converter for Fuel Cell Systems, *IEEE Transactions On Industry Applications*. 54 (2018) 665-674. doi:10.1109/tia.2017.2752686.

[26] M. Zandi, A. Payman, J. Martin, S. Pierfederici, B. Davat, F. Meibody-Tabar, Energy Management of a Fuel Cell/Supercapacitor/Battery Power Source for Electric Vehicular Applications, IEEE Transactions On Vehicular Technology. 60 (2011) 433-443. doi:10.1109/tvt.2010.2091433.

[27] R. Gavagsaz-Ghoachani, M. Phattanasak, J. Martin, B. Nahid-Mobarakeh, S. Pierfederici, P. Riedinger, Observer and Lyapunov-Based Control for Switching Power Converters With LC Input Filter, *IEEE Transactions On Power Electronics*. 34 (2019) 7053-7066. doi:10.1109/tpel.2018.2877180.

[28] S. Lee, S. Jung, Practical Implementation of a Factorized All Pass Filtering Technique for Non-minimum Phase Models, *International Journal Of Control, Automation And Systems*. 16 (2018) 1474-1481. doi:10.1007/s12555-017-0687-9.

[29] L. Gil-Antonio, B. Saldivar, O. Portillo-Rodriguez, G. Vazquez-Guzman, S. De Oca-Armeaga, Trajectory Tracking Control for a Boost Converter Based on the Differential Flatness Property, *IEEE Access*. 7 (2019) 63437-63446. doi:10.1109/access.2019.2916472.

[30] J. Garcia-Sanchez, E. Hernandez-Marquez, J. Ramirez-Morales, M. Marciano-Melchor, M. Marcelino-Aranda, H. Taud et al., A Robust Differential Flatness-Based Tracking Control for the "MIMO DC/DC Boost Converter–Inverter–DC Motor" System: Experimental Results, *IEEE Access*. 7 (2019) 84497-84505. doi:10.1109/access.2019.2923701.

[31] P. Thounthong, S. Sikkabut, P. Mungporn, L. Piegari, B. Nahid-Mobarakeh, S. Pierfederici et al., DC Bus Stabilization of Li-Ion Battery Based Energy Storage for a Hydrogen/Solar Power Plant for Autonomous Network Applications, *IEEE Transactions On Industry Applications*. 51 (2015) 2717-2725. doi:10.1109/tia.2015.2388853.

[32] A. De Bernardinis, M. Péra, J. Garnier, D. Hissel, G. Coquery, J. Kauffmann, Fuel cells multi-stack power architectures and experimental validation of 1kW parallel twin stack PEFC generator based on high frequency magnetic coupling dedicated to on board power unit, Energy Conversion And Management. 49 (2008) 2367-2383. doi:10.1016/j.enconman.2008.01.022.

[33] M. Fliess, J. Lévine, P. Martin, P. Rouchon, Flatness and defect of non-linear systems: introductory theory and examples, *International Journal Of Control*. 61 (1995) 1327-1361. doi:10.1080/00207179508921959.

[34] S. Sriprang, B. Nahid-Mobarakeh, N. Takorabet, S. Pierfederici, N. Bizon, P. Kuman et al., Permanent Magnet Synchronous Motor Dynamic Modeling with State Observer-based Parameter Estimation for AC Servomotor Drive Application, *Applied Science And Engineering Progress*. 12 (2019). doi:10.14416/j.asep.2019.11.001.

[35] P. Thounthong, L. Piegari, S. Pierfederici, B. Davat, Nonlinear intelligent DC grid stabilization for fuel cell vehicle applications with a supercapacitor storage device, *International Journal Of Electrical Power & Energy Systems*. 64 (2015) 723-733. doi:10.1016/j.ijepes.2014.07.061.

[36] W. Thammasiriroj, V. Chunkag, M. Phattanasak, S. Pierfederici, B. Davat, P. Thounthong, Nonlinear single-loop control of the parallel converters for a fuel cell power source used in DC grid applications, *International Journal Of Electrical Power & Energy Systems*. 65 (2015) 41-48. doi:10.1016/j.ijepes.2014.09.025.

[37] P. Thounthong, S. Sikkabut, N. Poonnoy, P. Mungporn, B. Yodwong, P. Kumam et al., Nonlinear Differential Flatness-Based Speed/Torque Control With State-Observers of Permanent Magnet Synchronous Motor Drives, *IEEE Transactions On Industry Applications*. 54 (2018) 2874-2884. doi:10.1109/tia.2018.2800678.

[38] P. Mungporn, P. Thounthong, S. Sikkabut, B. Yodwong, C. Ekkaravarodome, P. Kumam et al., Differential Flatness-Based Control of Current/Voltage Stabilization for a Single-Phase PFC with Multiphase Interleaved Boost Converters, *2017 European Conference On Electrical Engineering And Computer Science (EECS)*. (2017). doi:10.1109/eecs.2017.32.

[39] G. Escobar, A. J. van der Schaft, R. Ortega, A Hamiltonian viewpoint in the modeling of switching power converters, *Automatica*, 35 (1999) 445-452. Doi: 10.1016/S0005-1098(98)00196-4.

[40] P. Mungporn *et al*., "Modeling and Control of Multiphase Interleaved Fuel-Cell Boost Converter based on Hamiltonian Control Theory for Transportation Applications," *IEEE Transactions on Transportation Electrification*, in press 2020, doi: 10.1109/TTE.2020.2980193.

[41] P. Thounthong, S. Pierfederici, B. Davat, Analysis of Differential Flatness-Based Control for a Fuel Cell Hybrid Power Source, *IEEE Transactions On Energy Conversion*. 25 (2010) 909-920. doi:10.1109/tec.2010.2053037.

Phatiphat Thounthong was born in Phatthalung, Thailand, on December 29, 1974. He received the B.S. and M.E. degrees in electrical engineering from King Mongkut's Institute of Technology North Bangkok (KMITNB), Bangkok, Thailand, in 1996 and 2001, respectively, and the Ph.D. degree in electrical engineering from Institut National Polytechnique de Lorraine (INPL)-Université de Lorraine, Nancy-Lorraine, France, in 2005.

Since 2012, he has been a Full Professor in Department of Teacher Training in Electrical Engineering, King Mongkut's University of Technology North Bangkok. He is the author of 142 scientific papers (including 23 papers in IEEE Transactions/Magazines) published in Scopus with citations = 3,217 times, H-index= 29, and G-index = 50. His current research interests include power electronics, electric drives, electric vehicles, electrical devices (fuel cells, photovoltaic, wind turbine, batteries, and supercapacitors), nonlinear controls, and observers.

Dr. Thounthong received the First Prize Paper Award from the IEEE Industry Applications Society-Industrial Automation and Control Committee in 2009 (Texas, USA), the Third Prize Outstanding Paper Award from the IEEE International Telecommunications Energy Conference in 2015 (Japan), the Best Poster Presentation Award from the IEEE International Conference on Electrical Machines in 2010 (Rome, Italy), the 2012 the Thailand Research Fund (TRF)-Commission on Higher Education (CHE)-**Scopus** Young Researcher Awards (Engineering and Multidisciplinary Technology) (https://www.elsevier.com/about/press-releases/science-and-technology/elsevier-announces-winners-of-2012-trf-che-scopus-researcher-awards-in-thailand), and the 2017 TRF-CHE-**Scopus** Researcher Awards (Engineering and Multidisciplinary Technology) (http://rescom.trf.or.th/display/keydefaultp.aspx?id_colum=230).

Pongsiri Mungporn received the B.S. and M.E. degrees in electrical engineering from the King Mongkut's University of Technology North Bangkok (KMUTNB), Bangkok, Thailand, in 2008 and 2016, respectively.

He is currently a Researcher with the Thai-French Innovation Institute, KMUTNB. He is the author of 28 scientific papers (including 4 papers in IEEE Transactions) published in Scopus with citations = 147 times, H-index= 5. His current research interests include power electronics, and electrical devices (fuel cells, solar cell, batteries, and supercapacitors).

Damien Guilbert was born in Paris, France, in 1987. He received the M.Sc. degree in electrical engineering and control systems and the Ph.D. degree in electrical engineering from the University of Technology of Belfort-Montbéliard (UTBM), France, in 2011 and 2014 respectively. He was involved in the creation of the first IEEE/IAS student branch and chapter in France at UTBM. Since September 2016, he has been Associate Professor at Université de Lorraine and a permanent member of GREEN (Group of Research in Electrical Engineering of Nancy) laboratory.

His current research interests include power electronics, fuel cell and electrolyzer system, modeling and emulation of PEM electrolyzers, fault-tolerant DC/DC converters for fuel cell/photovoltaic/electrolyzer applications, fault-tolerant

control for fuel cell/electrolyzer systems and energy management of multi-source systems based on renewable energy sources and hydrogen buffer storage.

Noureddine Takorabet received the Engineering degree from the Ecole Nationale Polytechnique d'Alger, El Harrach, Algeria, in 1993, the Master's degree in electrical engineering from the University Nancy I, Nancy, France, in 1994, and the Ph.D. degree from the Université de Lorraine, Nancy, France, in 1996.

He is currently a Professor with the Université de Lorraine, where he is a member of the Groupe de Recherche en Électrotechnique et en Électronique de Nancy (GREEN), École Nationale Supérieure d'Électricité et de Mécanique, Université de Lorraine. His teaching activities concern electrical machines, electromagnetics, and the numerical simulation and design of electromagnetic devices. His main research activities include the modeling and optimization of electromagnetic devices, particularly electromechanical conversion.

Serge Pierfederici received the Dipl.-Ing. Degree in electrical engineering from the École Nationale Supérieure d'Électricité et de Mécanique, Institut National Polytechnique de Lorraine (INPL), Nancy, France, in 1994, and the Ph.D. degree from INPL in 1998.

Since 2009, he has been a Full Professor with the Université de Lorraine, Nancy. He has authored or coauthored more than 250 international peer-reviewed journals and conference articles, several book chapters, and holds several patents. His current research interests include the stability study of distributed power system, the control of dc and ac microgrids, and the design of power electronic converters for specific applications, such as fuel cells and electrolyser systems.

Babak Nahid-Mobarakeh received the Ph.D. degree in electrical engineering from the Institut National Polytechnique de Lorraine (INPL), Nancy, France, in 2001. From 2001 to 2006, he was at the Centre de Robotique, Electrotechnique et Automatique, University of Picardie, Amiens, France. In September 2006, he joined the Ecole Nationale Superieure d'Electricite et de Mecanique, University of Lorraine, Nancy, where he worked as a Professor until December 2019. Since January 2020, he is a Professor at McMaster University, Hamilton, Canada.

Dr. Nahid-Mobarakeh is the author or coauthor of more than 250 international peer reviewed journal and conference papers as well as several book chapters and patents. He has been the recipient of several IEEE awards. Dr. Nahid-Mobarake his the General Chair of the 2020 IEEE Transportation Electrification Conference and Expo (ITEC). Between 2012 and 2019, he served as Secretary, Vice Chair, Chair and Past Chair of the Industrial Automation and Control Committee (IACC) of the IEEE Industry Applications Society (IAS). He also was the IACC Committee Administrator and TCPRC. His main research interests include nonlinear and robust control design of power converters and drives, fault detection and fault-tolerant control of electric systems, and design, control and stabilization of microgrids.

Yihua Hu received the B.S. degree in electrical engineering and the Ph.D. degree in power electronics and drives from the China University of Mining and Technology, Xuzhou, China, in 2003 and 2011, respectively. From 2011 to 2013, he was with the College of Electrical Engineering, Zhejiang University, Hangzhou, China, as a Post-Doctoral Fellow.

From 2013 to 2015, he worked as a Research Associate with the Power Electronics and Motor Drive Group, University of Strathclyde, Glasgow, U.K. From 2016 to 2019, he was a Lecturer with the Department of Electrical Engineering and Electronics, University of Liverpool (UoL), Liverpool, U.K. He is currently a Reader with the Electronics Engineering Department, University of York (UoY), York, U.K. He has published 100 articles in the IEEE TRANSACTIONS journals. His research interests include renewable generation, power electronics converters and control, electric vehicle, more electric ship/aircraft, smart energy systems, and nondestructive test technology.

Nicu Bizon was born in Albesti de Muscel, Arges county, Romania, 1961. He received the B.S. degree in electronic engineering from the University "Polytechnic" of Bucharest, Romania, in 1986, and the PhD degree in Automatic Systems and Control from the same university, in 1996.

From 1996 to 1989, he was in hardware design with the Dacia Renault SA, Romania. He is currently professor with the University of Pitesti, Romania. He received two awards from Romanian Academy, in 2013 and 2016. He is editor of ten books and more than 500 papers in scientific fields related to Energy (from these 115 papers are indexed in WOS (39 Q1; 2 Q2; 2 Q3; 2 Q4; 56 in conferences; 21 chapters); H-index WOS = 21). His current research interests include power electronic converters, fuel cell and electric vehicles, renewable energy, energy storage system, microgrids, and control and optimization of these systems.

Yigeng Huangfu received the master's and Ph.D. degrees in electrical engineering from Northwestern Polytechnical University (NPU), Xi'an, China, in 2007 and 2009, respectively. He also received the Ph.D. degree from the University of Technology of Belfort-Montbéliard (UTBM), Belfort, France, in 2010.

Between 2009 and 2013, hewas a Lecturerwith the School of Automation at NPU, where he is currently an Associate Professor and a Ph.D. Tutor. Dr. Huangfu serves as Secretary General of the Technical Committee on Transportation Electrification of the IEEE Industry Electronic Society. He is an Associate Editor for IEEE INDUSTRIAL ELECTRONICS TECHNOLOGY NEWS (ITeN), IEEE JOURNAL OF EMERGING AND SELECTED TOPICS IN INDUSTRIAL ELECTRONICS, and IET Power Electronics.

Poom Kumam received the B.S. degree in mathematics from Burapha University, Thailand, in 2000, the M.Sc. degree in mathematics from Chiang Mai University, Chiang Ma, Thailand, in 2002, and Ph.D. degree in mathematics from Naresuan University, Phitsanulok, Thailand, in 2007. Dr.Kumam is a full Professor in the Department of Mathematics, Faculty of Science, Mongkut's University of Technology Thonburi (KMUTT), Thailand since 2015. He is the head of the Theoretical and Computational (TaCS) Center and KMUTT Fixed Point Theory and Applications Research Group.

His research targeted fixed-point theory, variational analysis, random operator theory, optimization theory, and approximation theory. Also, Fractional differential equations, Differential game, Entropy and Quantum operators, Fuzzy soft set, Mathematical modelling for fluid dynamics and areas of interest Inverse problems, Dynamic games in economics, Traffic network equilibria, Bandwidth allocation problem, Wireless sensor network, Image restoration, Signal and image processing, Game Theory and Cryptology. He has provided and developed many mathematical tools in his fields productively over the past years. Dr. Poom has over 600 scientific papers and projects either presented or published. Moreover, he is editorial board

journals more than 40 journals and also he delivers many invited talks on different international conferences every year all around the world.

@@@ END @@@